

Evaluation of the Unsteady Turbulence Modelling and Thermal Insulation on the Performance of Partial Combustion Lance

Woon Phui Law^a, Jolius Gimbun^{*b}

^aFaculty of Chemical & Natural Resources Engineering, Univ. Malaysia Pahang, 26300 Gambang, Pahang, Malaysia

^bCentre of Excellence for Advanced Research in Fluid Flow, Univ. Malaysia Pahang, 26300 Gambang, Pahang, Malaysia

jolius@ump.edu.my

A computational fluid dynamics (CFD) study of a partial combustion lance (PCL) was performed using a hybrid scale adaptive simulation (SAS) in this work. In addition, the unsteady Reynolds-averaged Navier-Stokes (URANS) simulations using the standard $k-\epsilon$ (SKE), realizable $k-\epsilon$ (RKE) and renormalized (RNG) $k-\epsilon$ were performed for comparison purpose. Combustion was modelled using the species transport model, whereas the heat transfer was calculated using a combined convection-radiation boundary condition. Suitability of various gradient methods (i.e., Green-Gauss node-based, Green-Gauss cell-based and least squares cell-based) to discretize the convection and diffusion terms in the governing equations were assessed by comparing the CFD prediction with experimentally measured temperature. It was found that SAS provided a better prediction of the PCL temperature with about 5.1 % of error from the experimental data. The Green-Gauss node-based method showed a better agreement compared to the two cell-based gradient methods. Installation of thermal insulation increased the peak temperature by about 9.4 %. The finding in this work indicated that CFD model is useful for retrofitting study of an existing PCL.

1. Introduction

Partial combustion of syngas is defined as an oxidation process which is often used for iron reduction in steel manufacturing plant. The type of thermal insulation used to minimize the heat loss may affect the performance of a partial combustion lance (PCL) (Nicolau and Dadam, 2009). Heat loss is an important issue in the partial combustion system (Filkoski et al., 2013). Minimal energy waste and reduced fuel consumption can be achieved in an insulated system (Nicolau and Dadam, 2009).

The turbulent flow in PCL caused the velocity and pressure fluctuates chaotically, together with the transport quantities, e.g., mass, momentum and energy. Turbulence induces intense mixing of species involved in the combustion process promoting a faster reaction hence a better combustion. Therefore, it is important to model the turbulent flow inside the PCL accurately. Ideally, experimental measurement is needed to understand the complex behaviour of the reactive and turbulence flow inside the PCL. However, experimental measurement (i.e., particle image velocimetry (PIV) and laser doppler velocimetry (LDV)) has various limitations such as high operating cost, not applicable to opaque wall and dangerous to be conducted at high operating temperature. Thus, computational fluid dynamics (CFD) is often used as an alternative method to obtain the fluid flow and combustion characteristic in a combustion chamber.

In previous works, unsteady Reynolds-averaged Navier-Stokes (URANS) model and large eddy simulation (LES) were mostly used to predict the turbulent flow in PCL. However, URANS model has intrinsic limitations to model turbulent flow due to the anisotropic nature of turbulence, while the computational cost of LES does not differ appreciably to that of direct numerical simulation (DNS) in the boundary layer region (Spalart, 2000). Alternatively, the hybrid scale adaptive simulation (SAS) can be employed since it offers an anisotropic perspective of turbulent flow and least sensitive to computational grid, unlike the LES (Menter and Egorov, 2006). To our best knowledge, SAS model has never been employed to study the

reactive flow in PCL previously; hence this is the aim of this work. In addition, the URANS using various $k-\epsilon$ derivatives such as standard $k-\epsilon$ (SKE), realizable $k-\epsilon$ (RKE) and renormalized (RNG) $k-\epsilon$ was performed for comparison purpose. The effect of three gradient methods, i.e., Green-Gauss node-based (GGNB), Green-Gauss cell-based (GGCB) and least square cell-based (LSCB) on the prediction accuracy was evaluated. The predicted velocity and temperature were compared with the experimental data. The validated model was then used to evaluate the effect of thermal insulation on the temperature in the PCL.

2. Three-dimensional domain and grid

Figure 1 shows a PCL fitted with two oxygen lances and nozzles. The three-dimensional PCL geometry was created using ANSYS Gambit 2.4.6. The length of the PCL is 6.35 m and 1.266 m in diameter. Two oxygen lances are installed vertically at 1.35 m from the PCL inlet. Each oxygen lance has length of 0.483 m and 0.06 m in diameter, while the nozzle has 0.03 m of length and 0.022 m in diameter. The syngas enters into PCL at 1,203 K and 118 m/s, while pure oxygen is injected at 300 K and at 70 m/s through the nozzles. The composition of syngas is shown in Table 1. The PCL wall is made of 0.03 m thick steel with a convective heat transfer coefficient of 0.5 W/m²/K.

The PCL in this work is a part of a Tenova HYL direct reduction process which was installed between the process gas heater and oxide removal reactor, similar to the one studied by Zain et al. (2011). The gas composition at the PCL inlet was measured using a micro gas chromatography (Agilent GC 3000) and the temperature was measured using a type-K thermocouple. A molecular sieve column was used for analysis of hydrogen (H₂), methane (CH₄), oxygen (O₂), nitrogen (N₂) and carbon monoxide (CO) at 368 K, whereas the Plot U column was used for analysis of carbon dioxide (CO₂) at 373 K. A high purity (over 99.99 %) helium (He) gas was used as carrier gas. The type-K thermocouple has a measurement range from 73.15 K to 1,533.15 K and is suitable for use in an oxidizing environment. The type-K thermocouple has a tolerance of ± 2.5 K at temperature ranged from 233.15 K to 606.15 K and ± 0.0075 T K at the temperature ranged from 606.15 K to 1,473.15 K. The thermocouple was installed at a position of 5.85 m after the inlet, just before the oxide removal reactor (see Figure 1). The computational grid was prepared using the cut-cell method in ICFM CFD 15.0, which offers a robust and faster convergence compared to the traditional meshing technique (Ingram et al., 2003) while retaining the boundary conforming grid. The oxygen lance and nozzle region was meshed using finer mesh (8.4×10^{-7} m³ to 2.7×10^{-6} m³) while the bulk region was meshed using coarser meshes (1.8×10^{-5} m³ to 1.8×10^{-4} m³). About 434 thousands cells were employed to the whole PCL domain.

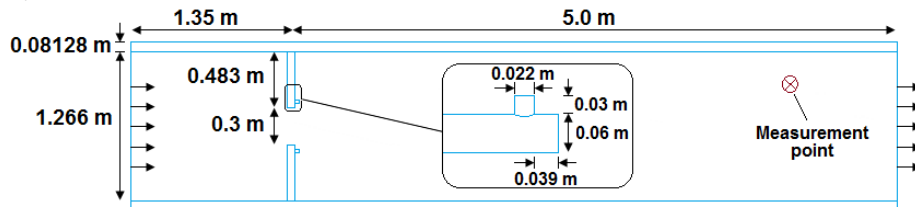


Figure 1: A schematic of PCL geometry. Measurement point is taken at a position of 5.85 m from PCL inlet and 0.373 m from centreline

Table 1: Mass fraction of syngas species at the PCL inlet

Species	CH ₄	CO	CO ₂	H ₂	H ₂ O	N ₂
Mass fraction	0.132	0.486	0.072	0.154	0.029	0.126

Table 2: Parameters for the five chemical reactions

No.	Chemical reaction	Rate order	Pre-exponential factor	Activation energy (J/kmol)
1	$CH_4 + 1.5O_2 \rightarrow CO + 2H_2O$	$[CH_4]^{0.7} [O_2]^{0.8}$	5.012×10^{11}	2.0×10^8
2	$CO + 0.5O_2 \rightarrow CO_2$	$[CO]^1 [O_2]^{0.25}$	2.239×10^{12}	1.7×10^8
3	$H_2 + 0.5O_2 \rightarrow H_2O$	$[H_2]^1 [O_2]^1$	9.87×10^8	3.1×10^7
4	$CH_4 + 2O_2 \rightarrow CO_2 + 2H_2O$	$[CH_4]^{0.2} [O_2]^{1.3}$	2.119×10^{11}	2.03×10^8
5	$CO_2 \rightarrow CO + 0.5O_2$	$[CO_2]^1$	5.0×10^8	1.7×10^8

3. Species transport modelling

The chemical reactions during the partial combustion in a PCL are shown in Table 2. Reactions 1 and 4 are the partial and complete combustion of CH₄; reactions 2 and 3 are the partial combustion of CO and H₂, and reaction 5 is the CO₂ dissociation. The partial combustion of syngas was modelled using a combination of finite rate and eddy dissipation model (EDM) which includes both Arrhenius and mixing rate, whereby the lower rate from either model dictates the reaction.

4. Heat transfer modelling

Radiation, conduction and convection occur simultaneously in a heat transfer system like the PCL. In an insulated PCL, radiation and conduction are the dominant heat transfer mechanisms while the convection effect is relatively small (Tleoubaev, 1998). The external convective heat transfer coefficient is negligible compared to the internal convective heat transfer coefficient, and hence excluded (Palmqvist, 2012). The rate of heat transfer is given by Eq (1):

$$\dot{Q} = \dot{Q}_{Rad} + \dot{Q}_{Cond} + \dot{Q}_{Conv} = \varepsilon\sigma(T_r^4 - T_s^4) + k(dT/dx) + h(T_g - T_s) \quad (1)$$

where \dot{Q} is the total heat transfer rate (W/m²), \dot{Q}_{Rad} is radiation rate (W/m²), \dot{Q}_{Cond} is conduction rate (W/m²), \dot{Q}_{Conv} is convection rate (W/m²), ε is emissivity of PCL wall, σ is Stefan-Boltzmann constant (W/m²/K⁴), k is thermal conductivity (W/m/K), x is insulator thickness (m), h is a convective heat transfer coefficient (W/m²/K), T_r is radiation temperature (K), T_s is wall surface temperature (K) and T_g is gas temperature (K).

5. Turbulence modelling

5.1 Reynolds-averaged Navier-Stokes model

Two-equation SKE is the most-used turbulence model owing to its simplicity, robustness and has a relatively low computational demand. As the shortcoming of SKE is known, an effort was made to introduce a turbulence model that takes into account the swirling effect as well as to ensure a realistic value (non-negative) for C_μ coefficient in k-equation (Shih et al., 1995). Unlike the SKE, C_μ coefficient in RKE is not constant and computed as a function of local states of the flow to ensure normal stresses are positive under all flow conditions. Therefore, this model can provide a better prediction on rotation and separation flows (Andersson et al., 2012). In RNG k- ε , the small-scale eddies are eliminated, and the transport coefficient is renormalized (Yakhot and Orszag, 1986). RNG differs from SKE because it has an analytical equation for turbulent Prandtl number (Pr_t) and additional term (R_ε) in ε -transport equation to account for the interaction between turbulence dissipation and mean shear. This additional term gives a slight reduction of dissipation rate, as the result reduces the effective viscosity. Thus, RNG k- ε model can provide better prediction for a region with large strain rate and streamline curvature.

5.2 Scale adaptive simulation model

RANS model gives a reasonable prediction for steady flows, but not ideal for the unsteady turbulence flows since it eliminates all turbulence scales from velocity field. Therefore, the SAS model which was first proposed by Rotta (1972) was introduced to overcome the RANS limitation. The original SAS model is developed based on exact transport equation for length scale and known as Rotta's KL model. The Rotta's KL model had been modified as two-equation model by Menter et al. (2006) and known as KSKL (K-square-root-K-L) model. A new ϕ model was used to replace the ψ model in the original Rotta's KL model

where $\phi = \sqrt{k}L$ and $\psi = kL$. The two equations in KSKL model are given as:

$$\frac{\partial}{\partial t}(\rho k) + \frac{\partial}{\partial x_i}(\rho u_i k) = P_k - C_\mu^{3/4} \rho \frac{k^2}{\phi} + \frac{\partial}{\partial x_i} \left[\left(\frac{\mu_t}{\sigma_k} \right) \frac{\partial k}{\partial x_i} \right] \quad (2)$$

$$\frac{\partial}{\partial t}(\rho \phi) + \frac{\partial}{\partial x_i}(\rho u_i \phi) = \frac{\phi}{k} P_k \left[\zeta_1 - \zeta_2 \left(\frac{L}{L_{vk}} \right)^2 \right] - \zeta_3 \rho k + \frac{\partial}{\partial x_i} \left[\left(\frac{\mu_t}{\sigma_\phi} \right) \frac{\partial \phi}{\partial x_i} \right] \quad (3)$$

where ρ is the density of fluid (kg/m³), k is turbulent kinetic energy (m²/s²), u is the velocity of fluid (m/s), P_k is the production term of turbulent kinetic energy, $\mu_t = C_\mu^{1/4} \rho \phi$ is turbulent viscosity (kg/m/s), L is turbulent

length scale and L_{vk} is the von Karman length scale. The model constant C_μ is 0.09, σ_k is 0.67, σ_Φ is 0.67, ζ_1 is 0.8, ζ_2 is 1.47 and ζ_3 is 0.0288 (Menter et al., 2006). $c_\mu^{1/4}$ corresponds to the turbulent length scale (L), which returns $L = ky$ in the logarithmic part of a near-wall boundary layer. The new Φ coefficient has an advantage of being directly proportional to the eddy viscosity and therefore allows formulation of one-equation model in addition to the proposed two-equation model. The addition of a new term, von Karman length scale, L_{vk} allows the SAS model to perform identically as a RANS model in steady-state flows and also applicable to unsteady-state flows by adjusting its length scale to resolve the turbulence spectrum in the unstable flows.

6. Numerical setting

The simulation of PCL was performed using ANSYS Fluent 15.0 installed on a HP Z220 workstation with Quadcore Xeon E3-1225 processor (3.2 GHz) and 8GB of RAM. The density, specific heat (Keenan et al., 1983), conductivity (Touloukian et al., 1970a) and viscosity (Touloukian et al., 1970b) of the syngas species from 123 K to 2,273 K were introduced as a piecewise linear function since their properties vary with temperature. The initial simulation was performed using a steady solver and first-order scheme, prior to the final simulation using the unsteady solver, standard pressure and second-order scheme, which yielded the best prediction of fluid flow in PCL (Law and Gimbut, 2014). The bounded central differencing was used to discretize the momentum equation and the bounded second-order implicit scheme was enabled for the SAS model. The properties of four different thermal insulators studied in this work are shown in Table 3.

Table 3: Properties of thermal insulators

Insulator	Density (kg/m^3)	Specific heat (J/kg/K)	Conductivity (W/m/K)	Emissivity	Reference
Brick	2,645	960	1.50	0.57	Nicolau and Dadam (2009)
Ceramic fibre	128	1,000	0.26	0.50	AAAMSA (2001)
Carbon felt	90	1,670	0.25	0.99	MorganAM&T, 2008
Graphite felt	80	1,670	0.43	0.99	MorganAM&T, 2008

7. Results and discussion

7.1 URANS and SAS

A comparison of the velocity and temperature prediction by the URANS and hybrid turbulence models (i.e., SKE, RKE, RNG $k-\epsilon$ and SAS) is shown in Figures 2(a) and 2(b). The simulation of an air flow past a cylindrical oxygen lance in a PCL at Reynolds number (Re) = 3,900 was compared with the PIV measurement by Lourenco and Shih (1993). The free-stream velocity (u_∞) of air was set to correspond to the subcritical Re of 3,900 to ensure a fair comparison with the experimentally measured velocity profile. Figure 2(a) demonstrated a normalized mean streamwise velocity ($u_x^* = u_x/u_\infty$) along the radial position (Z/D) at various axial sections (X/D). The data is taken at 0.4 m from the centreline of the PCL, which is 0.189 m away from the nozzle to avoid any flow disturbance. u_x is denoted as mean streamwise velocity, Z is radial position of PCL, X is axial position of PCL and D is the diameter of cylindrical oxygen lance. At $X/D = 1.06$, SAS showed a good agreement with the experimental velocity in the region of $-1.5 < Z/D < -0.5$ and $0.5 < Z/D < 1.5$. Whereas, URANS provided a better prediction than that SAS in the centre region ($-0.5 < Z/D < 0.5$). SAS provides better prediction on u_x^* than URANS away from the oxygen lance at $X/D = 3.00$. This finding showed that SAS accurately predicts the mean velocity in the PCL and the grid resolution in this work is adequate to capture the flow feature past the oxygen lance. Figure 2b showed the comparison of different turbulence models in predicting the temperature value near the outlet of the PCL. The SAS model yielded a good prediction with a deviation of 5.1 % from the experimental measurement (Zain et al., 2011). This may be attributed to the comprehensive modelling of turbulence length scale in SAS model. The SAS model account not only for the energy producing large eddies, but also resolved well the small eddies which are related to turbulence dissipation. The inclusion of von Karman length scale enables the SAS to model both steady and unsteady turbulence flow by allowing the formation of a broadband turbulence spectrum (Menter et al., 2006). In contrast, SKE, RKE and RNG $k-\epsilon$ are well suited for the wall-bounded flow (usually isotropic and low Re flows), and it may not accurately predict the larger-scale eddies, especially in the presence of a highly anisotropic turbulent flow. In this work, the cell Re ranged from 2.7×10^4 to 6.5×10^4 which falls under full turbulence region. In addition, the mixing and reaction just after the oxygen lances induced an unstable, high Re and larger scale eddy motion, which is

more suited for the LES model instead of the URANS model. Thus, SAS model was employed, which can switch to URANS mode near the boundary layer region and turn to LES mode in the bulk region by adjusting its length scale and providing a low enough eddy viscosity. Meanwhile, the three URANS models show larger errors, ranging from 5.7 % to 8.6 %. This finding suggests that a hybrid model (SAS) is more accurate than URANS model for reactive turbulence flow in PCL.

7.2 Gradient method

Three gradient methods (GGNB, GGCB and LSCB) were compared in this work using the SAS model. Figure 2c clearly showed that the prediction using GGNB method yields the lowest error (5.1 %) than other gradient method. The GGCB and LSCB methods showed a larger error of greater than 7 %. GGCB and LSCB compute the gradient values at the adjacent cell centroid. Whereas, GGNB computed the average values of nodes on the cell faces in a way that the second-order spatial accuracy is conserved, thus offers a more accurate prediction than the cell-based gradient method especially for an unstructured mesh although it requires longer computing time. The GGNB requires 3.49 s/iteration, whereas the GGCB and LSCB need 3.23 and 3.25 s/iteration. Therefore, since the computational effort is about the same, GGNB method was employed for the remainder of this work due to its accuracy.

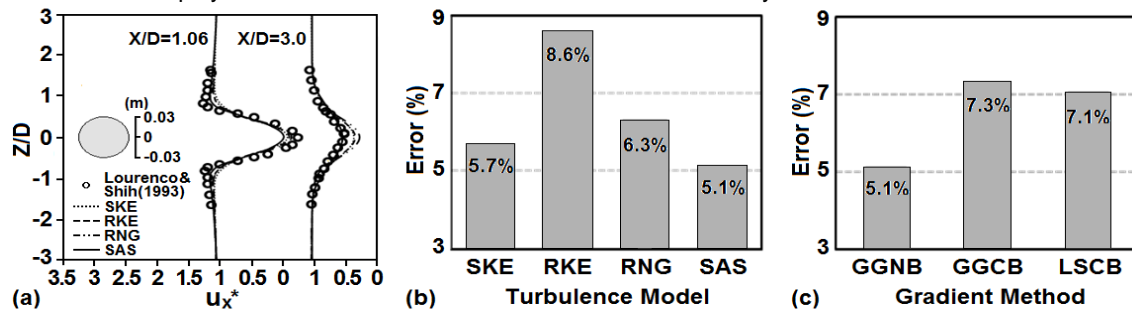


Figure 2: Comparison of turbulence models prediction for (a) u_x^* and (b) temperature; and (c) effect of gradient methods on temperature prediction. Data points for velocity measurement are adopted from Lourenco and Shih (1993). The error was calculated based on measurement by Zain et al. (2011)

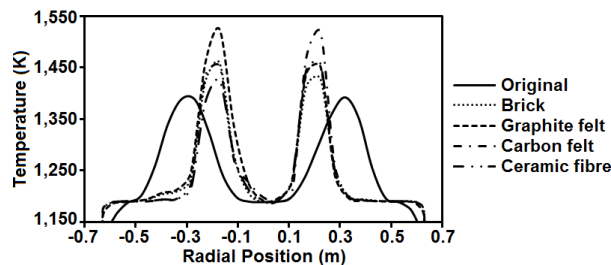


Figure 3: Effect of insulation on the predicted mean temperature in a PCL at $X = 5.85$ m from the PCL inlet

7.3 Thermal insulation

Four types of thermal insulators (i.e., brick, graphite felt, carbon felt and ceramic fibre) were considered in this work to minimise the heat loss from PCL. All design with thermal insulator was set to have a similar insulator wall thickness to ensure a fair comparison. The temperature profile in the PCL at a position of 5.85 m from the PCL inlet in the case with and without insulator is shown in Figure 3. The result shows a significant improvement in the combustion temperature for all the cases with insulator installed. A significant increase in the predicted peak temperature was observed for insulated PCL i.e., brick (4.8 %), graphite felt (9.4 %), carbon felt (9.1 %) and ceramic fibre (4.7 %). Four different insulation types showed a different peak temperature, mainly due to their physical properties. The highest emissivity of graphite and carbon felt is more efficient to emit back the thermal energy to the PCL and thus achieved higher combustion temperature compared to the brick and ceramic fibre (Viskanta and Grosh, 1962). Moreover, both graphite and carbon felt has a higher specific heat than both brick and ceramic fibre (Table 3), which gives a better ability of insulator to store the thermal energy (Singh et al., 2001). Hence, graphite and carbon felt achieved a higher improvement in the combustion temperature compared to that of brick and ceramic fibre. This work indicated that the insulation treatment by graphite felt achieved the best performance with 9.4 % higher peak temperature than the original design.

8. Conclusions

A comparison of the URANS and hybrid SAS models on the temperature prediction of a PCL was performed. This work found that SAS model yielded a better prediction with a deviation of 5.1 % from the experimentally measured temperature. The GGNB gradient method is best suited for an unstructured mesh in the PCL. The installation of thermal insulation showed improved performance where the graphite felt showed the highest improvement with about 9.4 % higher peak combustion temperature than the original design. The findings from this work may be useful for design retrofits of a PCL.

References

- Association of Architectural Aluminium Manufacturers of South Africa (AAAMSA), 2001, Thermal Insulation Handbook, <www.tiasa.org.za>, accessed 25.01.2014.
- Andersson B., Andersson R., Hakansson L., Mortensen M., Sudiyo R., Wachem B.V., 2012, Computational Fluid Dynamics for Engineers, Cambridge University Press, New York, USA. ISBN: 978-1-139-50556-7.
- Filkoski R.V., Bureskab L.J., Petrovski I.J., 2013, Assessment of the impact of under-fire air introduction on the pulverised coal combustion efficiency, Chemical Engineering Transactions, 34, 25-30.
- Ingram D.M., Causon D.M., Mingham C.G., 2003, Developments in Cartesian cut cell methods, Mathematics and Computers in Simulation, 61(3), 561-572.
- Keenan J.H., Chao J., Kaye J., 1983, Gas Tables, John Wiley and Sons, New York, USA.
- Law W.P., Gimbin J., 2014, A CFD study of a partial combustion lance, Proceedings of the 27th Symposium of Malaysian Chemical Engineers in conjunction with 21st Regional Symposium on Chemical Engineering (SOMChE & RSCE 2014), Subang, Malaysia.
- Lourenco L.M., Shih C., 1993, Characteristics of the plane turbulent near wake of a circular cylinder: A particle image velocity study (private communication), reported in Kravchenko A.G., Moin P., 2000, Numerical studies of flow over a circular cylinder at $Re_D=3900$, Physics of Fluids, 12(2), 403-417.
- Menter F.R., Egorov Y., 2006, SAS turbulence modelling of technical flows, In: Direct and large-eddy simulation VI, Eds. Lamballais E., Friedrich R., Guerts B.J., Metais O., Springer, Netherland, 687-694. ISBN: 978-1-4020-5152-2.
- Menter F.R., Egorov Y., Rusch D., 2006, Steady and unsteady flow modelling using the $k-\sqrt{k} L$ model, Proceedings of the Turbulence, Heat and Mass Transfer, 5, 403-406.
- MorganAM&T, 2008, Carbon and graphite felt insulation, <www.morganamt.com>, accessed 25.01.2014.
- Nicolau V.D.P., Dadam A.P., 2009, Numerical and experimental thermal analysis of a tunnel kiln used in ceramic production, Journal of the Brazilian Society of Mechanical Sciences and Engineering, 31(4), 297-304.
- Palmqvist O., 2012, Dynamic modelling of heat transfer processes in a supercritical steam power plant, MSc Dissertation, Chalmers University of Technology, Gothenburg, Sweden.
- Rotta J.C., 1972, Turbulent Flows (Turbulente Stromungen), 15, Teubner-Verlag, Stuttgart, Germany. ISBN: 978-3-322-91206-0.
- Shih T.H., Liou W.W., Shabbir A., Yang Z., Zhu J., 1995, A new $k-\epsilon$ eddy viscosity model for high Reynolds number turbulent flows, Computers Fluids, 24(3), 227-238.
- Singh P., Henneke M., Jayakaran J.D., Hayes R., Baukal C.E.Jr., 2001, Heat Transfer, In: The John Zink Combustion Handbook, Eds. Baukal C.E.Jr., CRC Press, Boca Raton, FL, USA. ISBN: 0-8493-2337-1.
- Spalart P.R., 2000, Strategies for turbulence modelling and simulation, International Journal of Heat and Fluids Flow, 21(3), 252-263.
- Tleoubaev A., 1998, Conductive and radiative heat transfer in insulators, Technical Report December, <www.lasercomp.com>, accessed 16.01.2015.
- Touloukian Y.S., Liley P.E., Saxena S.C., 1970a, Thermophysical Properties of Matter: Thermal Conductivity-Nonmetallic Liquids and Gases, 3, IFI/Plenum, New York, USA. ISBN: 0-306-67020-8.
- Touloukian Y.S., Saxena S.C., Hestermans P., 1970b, Thermophysical Properties of Matter: Viscosity, 11, IFI/Plenum, New York, USA. ISBN: 0-306-67031-3.
- Viskanta R., Grosh R.J., 1962, Effect of surface emissivity on heat transfer by simultaneous conduction and radiation, International Journal of Heat and Mass Transfer, 5, 729-734.
- Yakhot V., Orszag S.A., 1986, Renormalization group analysis of turbulence I: basic theory, Journal of Science Computing, 1(1), 3-51.
- Zain M.I.S., Gimbin J., Hassan Z., 2011, CFD study on the performance of oxygen lance for partial combustion unit at direct reduction plant, Proceedings of the 1st International Conference on Chemical Innovation, Terengganu, Malaysia, C160, <umpir.ump.edu.my/1697>, accessed 03.07.2015.